RESEARCH ARTICLE

Comparison of Two Finite-Permeability Subdomain Models for Surface-Mounted Permanent-Magnet Machines

CHE SUN[1], YOUTONG FANG[1,2], (Senior Member, IEEE), AND PIERRE-DANIEL PFISTER[1,2], (Member, IEEE)

[1]College of Electrical Engineering, Zhejiang University, Hangzhou 310027, China
[2]Zhejiang Provincial Key Laboratory of Electrical Machine Systems, Zhejiang University, Hangzhou 310027, China

Corresponding author: Pierre-Daniel Pfister (pierredaniel.pfister.public@gmail.com)

ABSTRACT Subdomain models have been widely used to quickly model the fields and the torque of surface-mounted permanent-magnet machines (SMPMMs). Nevertheless, when magnetic saturation occurs, those models which assume the permeability of the iron parts to be infinite tend to be inaccurate. More recently, two types of models have been developed that take the finite magnetic permeability of the machines into account, but a comparison of those models is still lacking. This article compares two finite-permeability subdomain models of SMPMMs. In the stator teeth and slots of the first model, boundary conditions are used in both radial and tangential directions. In the second model, the permeability change as a function of the angle in the stator slot and teeth is modeled using the Fourier series and the Cauchy product to solve Maxwell's equations. In this study, the calculation of two different SMPMMs shows that both models can handle machines with low and high numbers of teeth. This study shows that the error of the first model has a low sensitivity to iron permeability and parameter changes, while the accuracy of the second model heavily depends on the iron permeability and parameters. For a higher iron permeability, the second model is less accurate. Both models can achieve high prediction accuracy at a faster calculation speed than the finite element model. The first model needs only a few harmonics to have high accuracy.

INDEX TERMS Surface-mounted permanent-magnet machine, finite-permeability subdomain models, flux density, torque calculation, computation requirement.

I. INTRODUCTION

Surface-mounted permanent-magnet (PM) machines (SMPMMs) are widely used in many industrial applications for their simplicity of structure, high efficiency, power density, and torque density. To better design these machines for a specific application, using an accurate and computationally cheap mathematical motor model in the preoptimization process is often an efficient approach [1].

The finite element model (FEM) is a helpful tool for designing electrical machines because it can account for saturation and complex structures [2]. However, the disadvantage

The associate editor coordinating the review of this manuscript and approving it for publication was Philip Pong.

of the FEM is its relatively long computation time compared to the analytical models. This long computation time is a problem when many parameters need to be optimized. Maxwell-Fourier methods are very accurate analytical models. They have a good agreement with FEM, but most of these methods assume that the iron parts are infinitely permeable [3], [4], [5], [6], [7], [8]. Hence, they neglect the magnetic saturation effect and overestimate the magnetic flux and the electromagnetic torque.

Only a few articles on Maxwell-Fourier methods include the finite relative permeability of iron parts. The first introduction of iron parts in the magnetic field calculation by Maxwell-Fourier method is given in [9], which solves the partial differential equations (PDE) of the magnetic

vector potential in Cartesian coordinates. In [10], the same method is extended to the polar coordinate system. Roubache and Boughrara obtained the general solutions of Maxwell's equations by applying the principle of superposition and the interface conditions (ICs) in both θ-edge and r-edge directions [11]. In [12] and [13], this approach has been implemented to calculate the performance of spoke-type permanent-magnet machines. This approach is also applied in switched reluctance machines [14] and induction machines [15] to consider the finite permeability of iron parts.

Some other articles use the convolution theorem to consider the iron parts based on the Maxwell-Fourier methods. This approach was first proposed in [16]. The electrical machine is divided into an arbitrary number of homogeneous or non-homogeneous layers where the permeability in the stator or rotor slotting is represented as a Fourier series along the direction of permeability variation [17]. This approach has been applied with the non-linear soft magnetic material in switched reluctance machines [18], axial flux permanent-magnet machines [19], and synchronous reluctance machines [20]. In [21] and [22], the same method has also been applied in Halbach array permanent-magnet machines.

It is essential to understand better the performance differences associated with analytical models for infinite iron permeability, as it helps to choose the best model for a specific application [23]. This understanding of the differences is equally important for finite-permeability subdomain models (FPSMs). However, we have not found a discussion on the comparison between these FPSMs. In this article, we use the theories of [11] and [18] and apply them to SMPMMs. The model based on [11] is called here model I, and the model based on [18] is called model II. To the best of our knowledge, the theories of these two articles have not been fully applied to an SMPMM with an internal rotor. In [24], the theory of [11] has been applied in an SMPMM, but this paper only considers the machine in no-load operating conditions. The theory of [16] has been applied in an SMPMM with an outer rotor in [17].

From the ICs, a linear system is obtained. The size of the linear system's matrix varies depending on the number of ICs and the number of harmonics considered. The accuracy of the two models has been compared to FEM for one matrix size only [11], [16]. We did not find any articles that show the accuracy of those models compared to FEM for similar matrix size to give an in-depth perspective into the accuracy versus speed comparison of both models to FEM. In this article, we assess the accuracy of both two models for different calculation speeds and compare them to FEM.

In order to study the effect of different motor structures on the two models, two motors are chosen, one with fewer teeth and one with a higher number of teeth. Two machines are used to study the accuracy of predicting the magnetic flux density and the electromagnetic torque under different permeabilities for these two models. The influence of key parameters, such as the pole-arc-to-pole-pitch ratio and
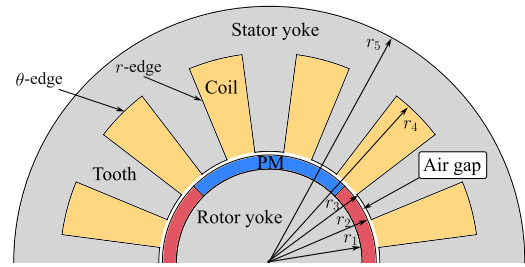

FIGURE 1. Structure of the SMPMMs.

slot-opening-to-slot-pitch ratio, on the average torque error is studied. Finally, we also study the relationship between matrix size and torque error. All results from these two models are compared with FEM with a very fine mesh.

II. FINITE-PERMEABILITY SUBDOMAIN MODELS
In this paper, the two analytical models are based on the following assumptions: 1) the magnetic permeability of the stator iron parts is finite, and the B-H curve is hence linear; 2) the stator teeth have no tooth-tips; 3) the PM poles are parallelly magnetized; 4) the end effect is negligible; 5) the stator slots/teeth have radial sides; 6) the permeability of rotor yoke is infinite.

A. MODEL I
In this model, the motor structure is divided into five types of subdomains: PMs, air gaps, stator slots, stator tooth, and stator yoke (Fig. 1). The general PDE of magnetic vector potential is derived from Maxwell's magnetostatic equations applied in different regions. The general solution for each region is obtained by using the separation of variables in PDE. The solutions of the magnetic vector potential in the air gap, the stator slots, the stator tooth, and the stator yoke, are given in [11]. The solutions of the magnetic vector potential A_z in the PMs are expressed by

$$A_{z1} = C_{10} + C_{20} \cdot \ln(r)$$
$$+ \sum_{n=1}^{\infty} [C_{1n} \cdot T_n + C_{2n} \cdot S_n + G_n] \cdot \sin(n\theta)$$
$$+ \sum_{n=1}^{\infty} [C_{3n} \cdot T_n + C_{4n} \cdot S_n + F_n] \cdot \cos(n\theta) \quad (1)$$

$$T_n = \left(\frac{r}{r_2}\right)^n \quad (2)$$

$$S_n = \left(\frac{r}{r_1}\right)^{-n} \quad (3)$$

$$G_n = (P_n(r) - P_{-n}(r))\,\iota \quad (4)$$

$$F_n = P_n(r) + P_{-n}(r), \quad (5)$$

where C_{10}, C_{20}, C_{1n}, C_{2n}, C_{3n} and C_{4n} are unknowns to be solved. The function $P_n(r)$ is the particular solution in the PM

TABLE 1. SMPMMs design parameters.

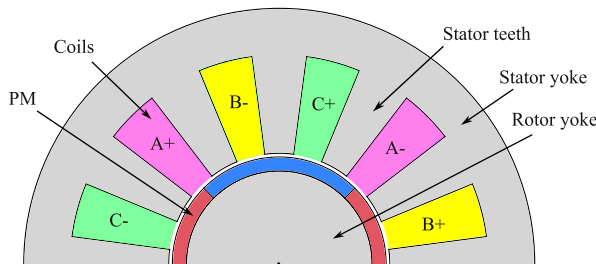| $2p/N_s$	4/12	16/36	Unit
PM inner radius r_1	20	126.7	mm
PM outer radius r_2	23	133.1	mm
Air gap outer radius r_3	23.8	134.2	mm
Slot outer radius r_4	45	158	mm
Stator outer radius r_5	55	169	mm
Current density J_{max}	2	1	A/mm^2
Pole-arc to pole-pitch ratio η	1	0.8	
Slot opening δ	15	5.4	degree
Active length l_a	100	140	mm
PM remanence B_R	1.1	1.32	T
PM relative permeability μ	1.1	1.05	

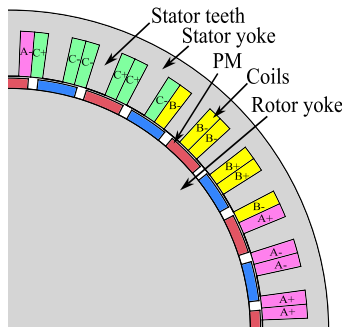**FIGURE 2.** Structure of machine I (4 poles/12 slots).

**FIGURE 3.** Structure of machine II (32 poles/36 slots).

region given by [8]

$$P_n(r) = \begin{cases} (\iota n B_{Rrn} - B_{R\varphi n}) \dfrac{r \ln(r)}{2} & n = \pm 1 \\ (\iota n B_{Rrn} - B_{R\varphi n}) \dfrac{r}{1-n^2} & n \neq \pm 1, \end{cases} \quad (6)$$

where B_{Rrn} and $B_{R\varphi n}$ are the harmonics of the remanent flux density given in [8].

Once the magnetic vector potential of each region is established, then the boundary conditions are applied to determine the constants. There are two types of ICs, along r-edges and θ-edges, respectively. In SMPMMs, the regions can be divided into two types: 1) periodic subdomains, such as PM, air gap, and stator yoke, and 2) non-periodic subdomains, such as stator slots and stator teeth. Both r-edges ICs and θ-edges ICs need to be considered in the non-periodic subdomain, while only θ-edges ICs need to be considered in the periodic subdomain. The boundary condition at the inner
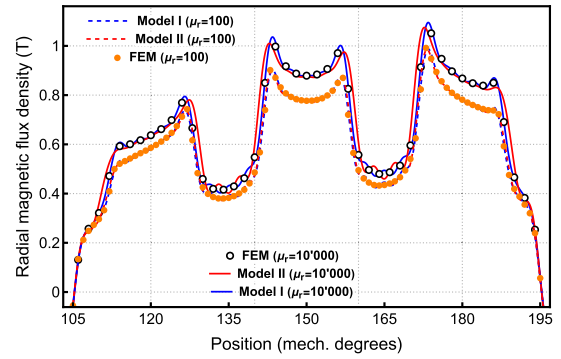
(a)
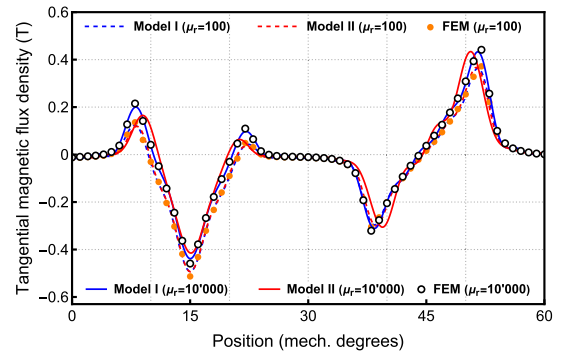
(b)

FIGURE 4. Air-gap magnetic flux density in the middle of the air gap of machine II: (a) radial and (b) tangential magnetic flux density.

radius of PM r_1 is [8]

$$\frac{1}{\mu_1}\left(\frac{\partial A_{z1}}{\partial r} + B_{R\varphi n}\right)\bigg|_{r_1} = 0. \quad (7)$$

The boundary conditions at the outer radius r_2 of the PM are

$$A_{z1}\,|_{r_2} = A_{z2}\,|_{r_2} \quad (8)$$

$$\frac{1}{\mu_1}\left(\frac{\partial A_{z1}}{\partial r} + B_{R\varphi n}\right)\bigg|_{r_2} = \frac{1}{\mu_0}\frac{\partial A_{z2}}{\partial r}\bigg|_{r_2}, \quad (9)$$

where μ_0 and μ_1 are vacuum and PM permeabilities, respectively. A_{z2} is the magnetic vector potential of the air gap.

The remaining boundary conditions are given in [11]. Finally, the unknowns can be determined by solving the linear system obtained from the ICs between various regions.

B. MODEL II

This model is valid only for homogeneous regions, so the SMPMMs are divided into different homogeneous regions. This model has a high level of convergence and describes the slotted machines using the Fourier series. The stator slots and tooth become a homogeneous region in this model, which differs from model I. Therefore, the SMPMMs are divided into four regions: I) PM region, II) air gap region, III) stator slots and tooth region, and IV) stator yoke region. The solution of
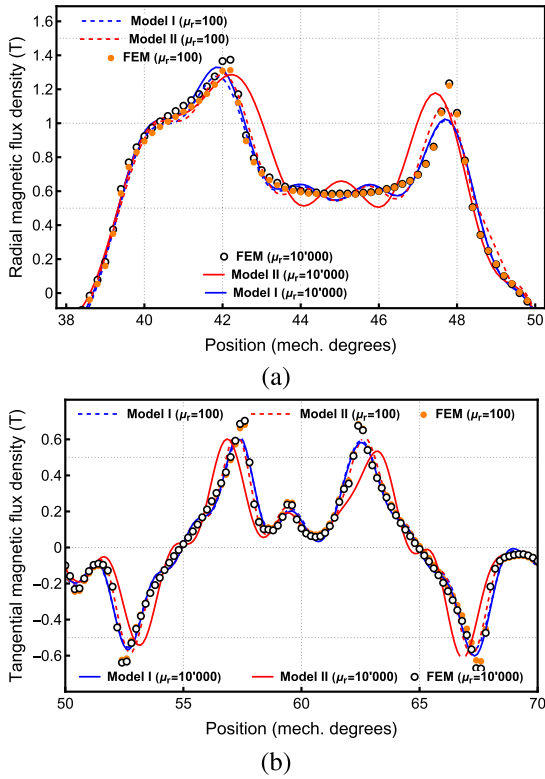
FIGURE 5. Air-gap magnetic flux density in the middle of the air gap of machine II: (a) radial and (b) tangential magnetic flux density.
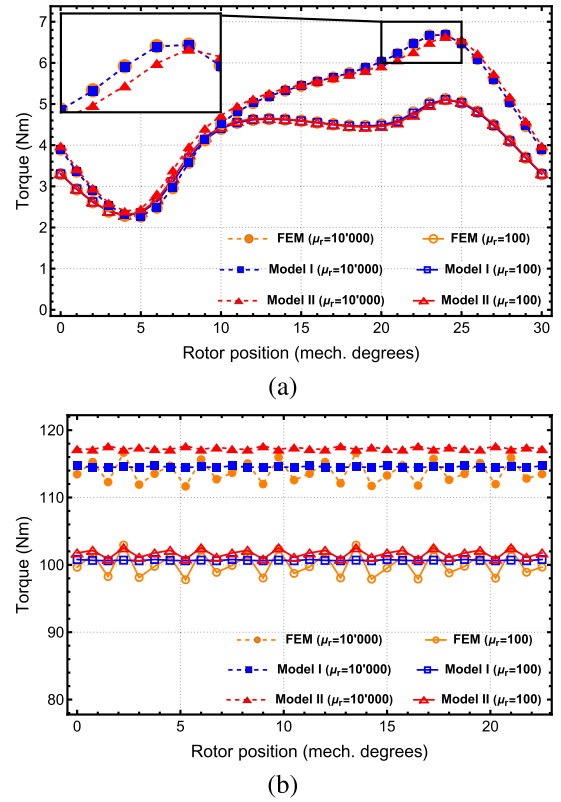

FIGURE 6. Electromagnetic torque waveforms: (a) machine I and (b) machine II.

each region is expressed as [18]

$$A_{z}^{I} |_r = \left(\frac{r}{r_2}\right)^{\lambda^{I}} a^{I} + \left(\frac{r_1}{r}\right)^{\lambda^{I}} b^{I} + G^{I} \qquad (10)$$

$$A_{z}^{II} |_r = \left(\frac{r}{r_3}\right)^{\lambda^{II}} a^{II} + \left(\frac{r_2}{r}\right)^{\lambda^{II}} b^{II} \qquad (11)$$

$$A_{z}^{III} |_r = W^{III} \left(\frac{r}{r_4}\right)^{\lambda^{III}} a^{III} + W^{III} \left(\frac{r_3}{r}\right)^{\lambda^{III}} b^{III} + r^2 F \qquad (12)$$

$$A_{z}^{IV} |_r = \left[\left(\frac{r}{r_5}\right)^{\lambda^{IV}} - \left(\frac{r_5}{r}\right)^{\lambda^{IV}}\right] a^{IV}, \qquad (13)$$

where λ and W are, respectively, the diagonal eigenvalue and the eigenvector matrix, and $r^2 F$ is the particular solution of region III [16]. The variables a and b are the column vectors of the constant unknown coefficients. The variable G is the particular solution of region I. In the SMPMMs, it can be written as

$$G^{I} = [P_{-N} (r) \cdots P_{N} (r)]^{T}, \qquad (14)$$

where N is the harmonic number of region I.

In model I, we need to consider both r-edges ICs and θ-edges ICs to obtain a linear system. However, we only need to consider θ-edges ICs in model II. On the interfaces between two regions, the boundary conditions are written as

$$A_{z}^{k} |_{r_i} = A_{z}^{k+1} |_{r_i} \qquad (15)$$

$$H_{\theta}^{k} |_{r_i} = H_{\theta}^{k+1} |_{r_i}, \qquad (16)$$

where H_{θ} is the tangential component of the magnetic field density, k represents the region, and r_i is the ith radius, for $i = 2$ to 4. The boundary conditions at the inner radius of PM r_1 is

$$H_{\theta}^{I} |_{r_1} = 0. \qquad (17)$$

The final linear system is solved for the unknowns a and b. We obtain A_z for all regions, which allows us to continue calculating magnetic flux density and electromagnetic torque.

III. COMPARISON OF THE TWO MODELS

The two FPSMs are compared for the flux density, electromagnetic torque, and the relationship between torque error and key parameters during the design process, such as the pole-arc-to-pole-pitch ratio and slot-opening-to-slot-pitch ratio, which will also be discussed further. Besides, the influence of the matrix size of both models on the torque error is also studied later. In order to study the relationship between the number of stator teeth and the number of harmonics, two machines are used, and their design parameters are shown in Table 1, with motor structures shown in Figs 2 and 3.

In order to make both models achieve high prediction accuracy for both machines, model I uses $n_{max} = 100$, $m_{max} = k_{max} = 10$ for machine I and $n_{max} = 200$, $m_{max} = k_{max} = 20$ for machine II, where n_{max}, m_{max} and k_{max} are the maximum
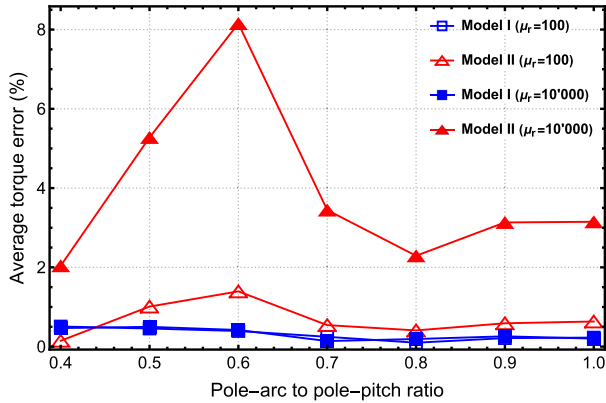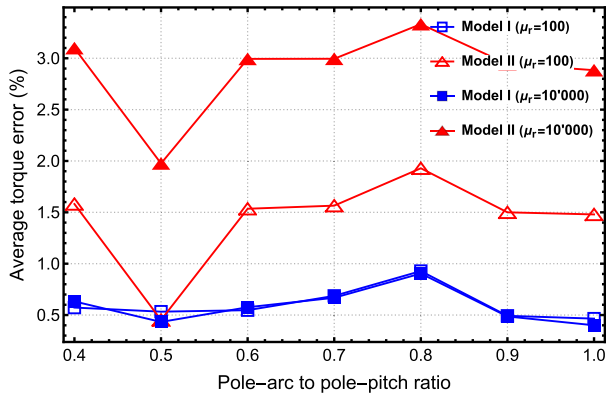
FIGURE 7. Average torque error against pole-arc-to-pole-pitch ratio of (a) machine I and (b) machine II, for a slot-opening-to-slot-pitch ratio of 0.5 for machine I, and 0.54 for machine II, respectively.

FIGURE 8. Average torque error against slot-opening-to-slot-pitch ratio of (a) machine I and (b) machine II, for a pole-arc-to-pole-pitch ratio of 1 for machine I and 0.8 for machine II, respectively.

numbers of harmonics in the periodic subdomains and the non-periodic subdomain, respectively [11]. Model II uses $N_{max} = 100$ for machine I and $N_{max} = 200$ for machine II, where N_{max} is the maximum number of harmonics in the homogeneous region [16]. We take FEM with fine mesh as a reference.
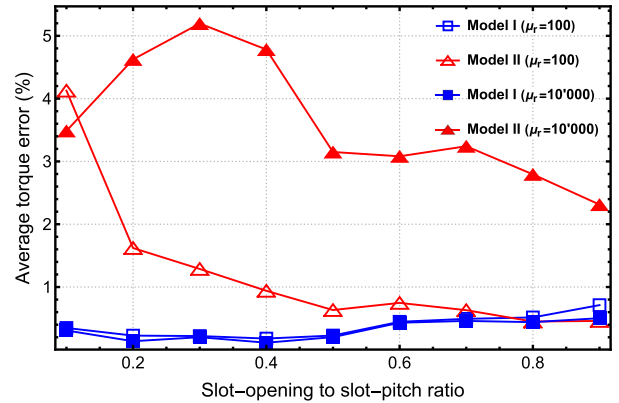
A. AIR-GAP FLUX DENSITY

The radial and tangential components of flux density in air-gap are given by

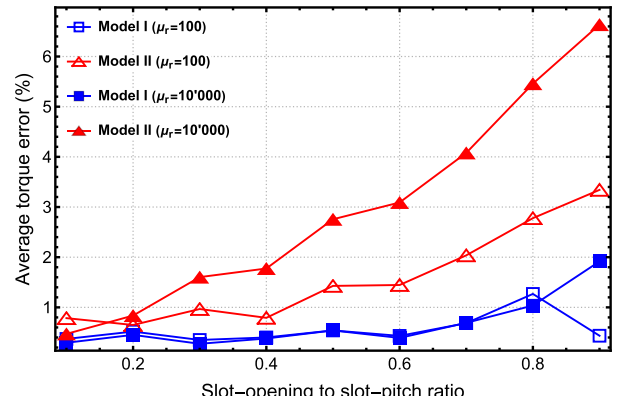$$B_r = \frac{1}{r}\frac{\partial A_z}{\partial \theta} \tag{18}$$

$$B_\theta = -\frac{\partial A_z}{\partial r}. \tag{19}$$

The air-gap flux density waveforms predicted by the two analytical models are compared with FEM results in Figs 4 and 5.

In order to fully demonstrate the impact of changes in the permeability of iron on the results, calculations using a relative permeability of 100 and 10'000 for the stator teeth and stator yoke are performed. The matrix size of fine mesh here is $36'916 \times 36'916$. From the results in Figs 4 and 5, it can be seen that the predicted magnetic flux density of both models, whether radial or tangential flux density, have a

good agreement with the FEM results when the iron relative permeability is 100. The relative error of radial flux density in model I is 1.39% for machine I and 3.14% for machine II, and the relative error of radial flux density in model II is 1.79% for machine I and 2.26% for machine II. When the iron relative permeability is 10'000, model I still has a good agreement with FEM. However, model II has some deviations from FEM. Indeed, the relative error of radial flux density in model I is 1.43% for machine I and 3.49% for machine II. In comparison, the relative error of radial flux density in model II is 5.02% for machine I and 14.35% for machine II.

B. ELECTROMAGNETIC TORQUE

The electromagnetic torque is calculated using Maxwell's stress tensor [25]:

$$T = \frac{l_a r^2}{\mu_0}\int_0^{2\pi} B_r B_\theta\, d\theta, \tag{20}$$

where l_a is the active length.

The fine mesh matrix size was, on average, around $37'000 \times 37'000$ here. The torque waveforms predicted by the two analytical models are compared with the FEM results in Fig. 6. When the stator iron relative permeability is 100, the torque pulsation of the two models matches very well with the results of the FEM, and the relative error of torque in
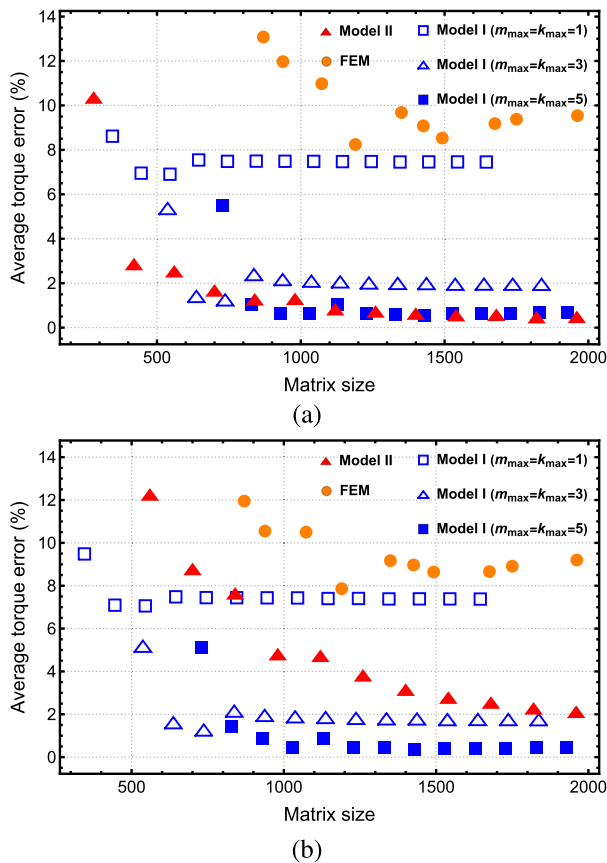
FIGURE 9. Average torque error for different divisions in model I and model II as a function of the matrix size for machine I, with (a) $\mu_r = 100$, and (b) $\mu_r = 10'000$. The pole-arc-to-pole-pitch ratio is 1, and the slot-opening-to-slot-pitch ratio is 0.5.

model I is 0.23% for machine I and 1.64% for machine II and the relative error of torque in model II is 0.78% for machine I and 1.73% for machine II. However, when the stator iron relative permeability is 10'000, model I still has high accuracy compared with FEM. In contrast, model II has some errors compared with FEM. The relative error of torque in model I is 0.20% for machine I and 1.37% for machine II while the relative error of torque in model II is 3.50% for machine I and 3.12% for machine II.

C. RELATIONSHIP BETWEEN TORQUE ERROR AND KEY PARAMETERS

The key parameters chosen here are pole-arc-to-pole-pitch ratio and slot-opening-to-slot-pitch ratio, which are critical parameters during the motor design process. The waveforms of average torque error against two parameters predicted by the two analytical models are shown in Figs 7 and 8, respectively. We can see that model I has higher accuracy for two different iron permeabilities and different key parameters. Its error is below 1% for different pole-arc-to-pole-pitch ratios and below 2% for different slot-opening-to-slot-pitch ratios under two different iron permeabilities.

We can also see that model II is very sensitive to parameter changes, and different key parameters can significantly affect the error of model II. For example, the maximum error is

8%, and the lowest error is 2% for machine I for an iron relative permeability of 10'000 (Fig. 7), while model I's error is always below 1%. Model I has low sensitivity to parameter changes and thus has better stability.

D. RELATIONSHIP BETWEEN TORQUE ERROR AND MATRIX SIZE

The resolution of these two models and of FEM involves the calculation of a matrix. The matrix size directly affects the calculation speed. The larger the matrix size, the larger the computation time. For example, the computation time of model I is 0.10 s when the matrix size is about 1'000 for machine I for $\mu_r = 100$, but the computation time is 0.32 s for the same condition when the matrix size is about 2'000.

In order to verify the accuracy of these models, the calculated torque was compared with FEM with a very fine mesh. The torque results of FEM modeled with different mesh precisions for machines I and II were also compared with FEM with a fine mesh. The torque was calculated as an average torque between different rotor positions, for which the fine mesh matrix size was, on average, around $37'000 \times 37'000$ for machine I and $78'000 \times 78'000$ for machine II. The results are shown in Figs 9 and 10. First, all points calculated using FEM show more error than those calculated using the two models for a given matrix size for machine I. On average, for a given matrix size, these two models have higher accuracy than FEM for machine II. The figures also show that the FEM calculation exhibits some random errors in the torque calculation, while the two analytical models have good stability.

Both models converge very quickly, and both can get convergence errors in relatively smaller matrix sizes. For model I, different combinations of m_{max} and k_{max} will result in different torque error distributions, and the final convergence torque error will also be different. The convergence error of model I is more significant than that of model II for two machines when taking $m_{max} = k_{max} = 1$, and is smaller than that of model II when taking $m_{max} = k_{max} = 5$. It is not necessary to take m_{max} and k_{max} very large. It can be seen from the figures that the error is already very small when taking $m_{max} = k_{max} = 5$, and the convergence error is below 1% for machine I and below 2% for machine II.

The error results of model I are not significantly affected by the change of iron permeability. However, when the iron relative permeability is 100, the convergence error of model II is 0.48% for machine I and 1.92% for machine II while the convergence error is 2.12% for machine I and 3.33% for machine II when iron relative permeability is 10'000. We call convergence error the value of the error taking a large number of harmonics into account.

IV. DISCUSSION

Tables 2 and 3 show that the prediction accuracy of radial flux density and electromagnetic torque for model I is very accurate for the two machines under different iron permeabilities. However, the error of model II increases when the iron
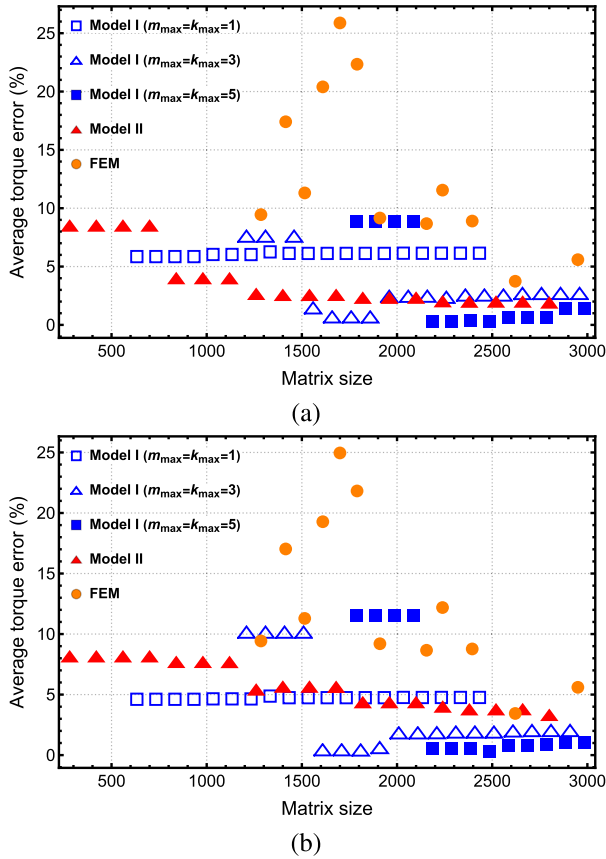
FIGURE 10. Average torque error for different divisions in model I and model II as a function of the matrix size for machine II, with (a) $\mu_r = 100$, and (b) $\mu_r = 10'000$. The pole-arc-to-pole-pitch ratio is 0.8 and the slot-opening-to-slot-pitch ratio is 0.54.

TABLE 2. The radial magnetic flux density error under different stator iron relative permeabilities for machines I and II.

Machine I				
Models	Model I	Model I	Model II	Model II
Relative permeability	100	10'000	100	10'000
Error	1.39%	1.43%	1.79%	5.02%
Machine II				
Relative permeability	100	10'000	100	10'000
Error	3.14%	3.49%	2.26%	14.35%

TABLE 3. The error of electromagnetic torque under different stator iron relative permeabilities for machines I and II.

Machine I				
Models	Model I	Model I	Model II	Model II
Relative permeability	100	10'000	100	10'000
Error	0.23%	0.20%	0.78%	3.50%
Machine II				
Relative permeability	100	10'000	100	10'000
Error	1.64%	1.37%	1.73%	3.12%

permeability increases. In Figs 7 and 8, we can also see that the error when the iron relative permeability is 100 is generally smaller than when the iron relative permeability is 10'000 for model II. Besides, when the iron relative permeability is 10'000, the convergence torque error of model II is bigger than the error when the iron relative permeability is 100 (Figs 9 and 10). As a comparison, model I is always very accurate for different iron permeabilities.

The reason for these errors is Gibbs phenomenon, which is the oscillatory behavior of the Fourier series of a periodic function around a jump discontinuity. In model II, the relative permeability in stator slots and teeth developed as a Fourier series expansion. Therefore the Gibbs phenomenon occurs at the boundary between the slot and the tooth. It is significant when the iron permeability is high. It contributes to the error and slows down the convergence. Because model I does not involve the expansion of iron permeability into the Fourier series in the tangential direction, it is not affected by the Gibbs phenomenon. It thus has high accuracy for any iron permeabilities.

The prediction accuracy of machine I is higher than machine II for these two models (Tables 2 and 3). The reason is that the structure of machine I has fewer teeth and pole pairs. Therefore it needs fewer harmonics. Higher harmonics are required for the calculation of machine II. If higher accuracy is required, the computation time increases considerably.

Tables 2 and 3 also show that electromagnetic torque's prediction accuracy is better than that of radial magnetic flux density for the two machines under different iron permeabilities overall. Indeed, the torque calculation intrinsically averages error circumferentially, whereas the magnetic flux densities are intrinsically local quantities. For torque calculation, a larger number of harmonics is unnecessary for a satisfactory error.

As mentioned in sections II-A and II-B, model I requires more boundary condition equations than model II to obtain the final linear system, so model I gives a more accurate description of the local magnetic field distribution than model II. It is the reason why model I is very accurate, but it is also the reason why it is more complex. The main advantage of model II is a good tradeoff between accuracy and complexity.

V. CONCLUSION
A comparative analysis of two FPSMs was performed on SMPMMs using FEM calculation with a fine mesh as a reference. Model I has a low sensitivity to the changes in iron permeability, while the accuracy of model II is very sensitive to iron permeability. As the iron permeability increases, the prediction accuracy of model II decreases, which is caused by the Gibbs phenomenon. Model I is accurate for different key parameters, while model II is more sensitive to parameter changes. Therefore, model II should be used with caution when studying magnetic saturation because it will give larger errors. In addition, model I is a better choice when optimizing some motor parameters as it has better stability.

Conversely, the final linear system formed by model I is more complex than that of model II, so if simplicity is favored, model II should be chosen. Model I is more accurate but at the cost of a greater minimum matrix size. If the requirement for accuracy is not high, model II can give, in some cases, a better compromise between accuracy and computation time.

Both models can achieve high prediction accuracy at a faster calculation speed than FEM. Different combinations of harmonics will result in different torque error distributions in model I. Taking a very high number of harmonics is unnecessary for model I, and good results can be achieved with a relatively low number of harmonics.

REFERENCES

[1] K. Ramakrishnan, M. Curti, D. Zarko, G. Mastinu, J. J. Paulides, and E. A. Lomonova, "A comparison study of modelling techniques for permanent magnet machines," in *Proc. 11th Int. Conf. Ecol. Vehicles Renew. Energies (EVER)*, Apr. 2016, pp. 1–6.

[2] L. J. Wu, Z. Q. Zhu, D. A. Staton, M. Popescu, and D. Hawkins, "Comparison of analytical models of cogging torque in surface-mounted PM machines," *IEEE Trans. Ind. Electron.*, vol. 59, no. 6, pp. 2414–2425, Jun. 2012.

[3] Z. Q. Zhu, D. Howe, E. Bolte, and B. Ackermann, "Instantaneous magnetic field distribution in brushless permanent magnet DC motors. I. Open-circuit field," *IEEE Trans. Magn.*, vol. 29, no. 1, pp. 124–135, Jan. 1993.

[4] Z. Q. Zhu and D. Howe, "Instantaneous magnetic field distribution in brushless permanent magnet DC motors. II. Armature-reaction field," *IEEE Trans. Magn.*, vol. 29, no. 1, pp. 136–142, Jan. 1993.

[5] Z. Q. Zhu, D. Howe, and C. C. Chan, "Improved analytical model for predicting the magnetic field distribution in brushless permanent-magnet machines," *IEEE Trans. Magn.*, vol. 38, no. 1, pp. 229–238, Jan. 2002.

[6] B. L. J. Gysen, K. J. Meessen, J. J. H. Paulides, and E. A. Lomonova, "General formulation of the electromagnetic field distribution in machines and devices using Fourier analysis," *IEEE Trans. Magn.*, vol. 46, no. 1, pp. 39–52, Jan. 2010.

[7] P.-D. Pfister and Y. Perriard, "Slotless permanent-magnet machines: General analytical magnetic field calculation," *IEEE Trans. Magn.*, vol. 47, no. 6, pp. 1739–1752, Jun. 2011.

[8] P.-D. Pfister, X. Yin, and Y. Fang, "Slotted permanent-magnet machines: General analytical model of magnetic fields, torque, eddy currents, and permanent-magnet power losses including the diffusion effect," *IEEE Trans. Magn.*, vol. 52, no. 5, pp. 1–13, May 2016.

[9] F. Dubas and K. Boughrara, "New scientic contribution on the 2-D subdomain technique in Cartesian coordinates: Taking into account of iron parts," *Math. Comput. Appl.*, vol. 22, no. 1, p. 17, Feb. 2017.

[10] F. Dubas and K. Boughrara, "New scientific contribution on the 2-D subdomain technique in polar coordinates: Taking into account of iron parts," *Math. Comput. Appl.*, vol. 22, no. 4, p. 42, Oct. 2017.

[11] L. Roubache, K. Boughrara, F. Dubas, and R. Ibtiouen, "New subdomain technique for electromagnetic performances calculation in radial-flux electrical machines considering finite soft-magnetic material permeability," *IEEE Trans. Magn.*, vol. 54, no. 4, pp. 1–15, Apr. 2018.

[12] B. L. Chikouche and R. Ibtiouen, "Analytical approach for spoke-type permanent magnet machine including finite permeability of iron core," *COMPEL-Int. J. Comput. Math. Electr. Electron. Eng.*, vol. 39, no. 2, pp. 333–352, Jan. 2020.

[13] A. Jabbari and F. Dubas, "An improved model for performances calculation in spoke-type permanent-magnet machines considering magnetization orientation and finite soft-magnetic material permeability," *COMPEL-Int. J. Comput. Math. Electr. Electron. Eng.*, vol. 39, no. 6, pp. 1299–1314, Nov. 2020.

[14] M. B. Yahia, L. Roubache, Z. Djelloul-Khedda, K. Boughrara, F. Dubas, and R. Ibtiouen, "A 2-D exact subdomain technique in switched reluctance machines taking into account of finite soft-magnetic material permeability," in *Proc. Int. Conf. Electr. Sci. Technol. Maghreb (CISTEM)*, Oct. 2018, pp. 1–6.

[15] A. Mollaeian, A. Kundu, M. S. Toulabi, M. U. Thamm, S. Kim, J. Tjong, and N. C. Kar, "Fourier-based modeling of an induction machine considering the finite permeability and nonlinear magnetic properties," *IEEE Trans. Energy Convers.*, vol. 36, no. 4, pp. 3427–3437, Dec. 2021.

[16] R. L. J. Sprangers, J. J. H. Paulides, B. L. J. Gysen, and E. A. Lomonova, "Magnetic saturation in semi-analytical harmonic modeling for electric machine analysis," *IEEE Trans. Magn.*, vol. 52, no. 2, pp. 1–10, Feb. 2016.

[17] Z. Djelloul-Khedda, K. Boughrara, F. Dubas, A. Kechroud, and B. Souleyman, "Semi-analytical magnetic field predicting in many structures of permanent-magnet synchronous machines considering the iron permeability," *IEEE Trans. Magn.*, vol. 54, no. 7, pp. 1–21, Jul. 2018.

[18] Z. Djelloul-Khedda, K. Boughrara, F. Dubas, and R. Ibtiouen, "Nonlinear analytical prediction of magnetic field and electromagnetic performances in switched reluctance machines," *IEEE Trans. Magn.*, vol. 53, no. 7, pp. 1–11, Jul. 2017.

[19] B. Guo, Y. Du, Z. Djelloul-Khedda, F. Peng, J. Dong, Y. Huang, F. Dubas, and K. Boughrara, "Nonlinear semianalytical model for axial flux permanent-magnet machine," *IEEE Trans. Ind. Electron.*, vol. 69, no. 10, pp. 9804–9816, Oct. 2022.

[20] R. L. J. Sprangers, J. J. H. Paulides, B. L. J. Gysen, J. Waarma, and E. A. Lomonova, "Semianalytical framework for synchronous reluctance motor analysis including finite soft-magnetic material permeability," *IEEE Trans. Magn.*, vol. 51, no. 11, pp. 1–4, Nov. 2015.

[21] H. S. Zhang, Z. X. Deng, M. L. Yang, Y. Zhang, J. Y. Tuo, and J. Xu, "Analytical prediction of Halbach array permanent magnet machines considering finite tooth permeability," *IEEE Trans. Magn.*, vol. 56, no. 6, pp. 1–10, Jun. 2020.

[22] D. C. Teles, C. Chillet, L. Garbuio, and L. Gerbaud, "Convergence algorithm for a nonlinear subdomain model of a parallel Halbach permanent magnet synchronous motor," in *Proc. Int. Conf. Electr. Mach. (ICEM)*, Sep. 2022, pp. 178–184.

[23] K. Ramakrishnan, M. Curti, D. Zarko, G. Mastinu, J. J. H. Paulides, and E. A. Lomonova, "Comparative analysis of various methods for modelling surface permanent magnet machines," *IET Electr. Power Appl.*, vol. 11, no. 4, pp. 540–547, Apr. 2017.

[24] B. L. Chikouche, "Analytical model for PMSM analysis including finite soft-magnetic material permeability," in *Proc. 11th Int. Conf. Electr. Electron. Eng. (ELECO)*, Nov. 2019, pp. 200–204.

[25] Y. Oner, Z. Q. Zhu, L. J. Wu, X. Ge, H. Zhan, and J. T. Chen, "Analytical on-load subdomain field model of permanent-magnet vernier machines," *IEEE Trans. Ind. Electron.*, vol. 63, no. 7, pp. 4105–4117, Jul. 2016.
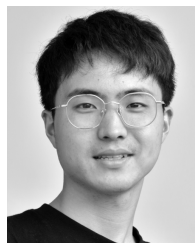
CHE SUN was born in Anhui, China, in 1999. He received the B.S. degree in electrical engineering from the Hefei University of Technology, Hefei, China, in 2021. He is currently pursuing the M.Sc. degree with Zhejiang University, Hangzhou, China.

His research interest includes the modeling and analysis of permanent-magnet machines.

YOUTONG FANG (Senior Member, IEEE) received the B.S. and Ph.D. degrees in electrical engineering from the Hebei University of Technology, Hebei, China, in 1984 and 2001, respectively.

Currently, he is a Professor with the College of Electrical Engineering, Zhejiang University, Hangzhou, China. His research interests include the application, control, and the design of electrical machines.

Dr. Fang achieved the Second Prize of the National Scientific and Technological Progress Award (twice), the First Prize of Provincial Science and Technology Progress Award (twice), and the First Prize of Provincial Science and Technology Progress Award (three times).

PIERRE-DANIEL PFISTER (Member, IEEE) was born in Bienne, Switzerland, in 1980. He received the M.Sc. and Ph.D. degrees in physics from the Swiss Federal Institute of Technology, Lausanne (EPFL), Switzerland, in 2005 and 2010, respectively.

He is currently an Associate Professor with Zhejiang University, Hangzhou, China. His current research interests include permanent-magnet machines, very-high-torque-density machines, analytical optimization, and robotics.

● ● ●